

Probing scattering of Raman phonons on magnetic and electronic excitations in pyrochlores $\text{Nd}_2\text{Zr}_2\text{O}_7$ and $\text{Nd}_2\text{Ir}_2\text{O}_7$.

Sami Muhammad,¹ Yuanyuan Xu,¹ Christos Kakogiannis,¹ Takumi Ohtsuki,² Yang Qiu,² Satoru Nakatsuji,^{2,3,4,5,6} Eli Zoghlin,⁷ Stephen D. Wilson,⁷ and Natalia Drichko¹

¹*Institute for Quantum Matter and Department of Physics and Astronomy,
Johns Hopkins University, Baltimore, Maryland 21218, USA*

²*Institute for Solid State Physics, University of Tokyo, Kashiwa, Chiba 277-8581, Japan*

³*Department of Physics, University of Tokyo, Bunkyo-ku, Tokyo 113-0033, Japan*

⁴*Institute for Quantum Matter and Department of Physics and Astronomy,
Johns Hopkins University, Baltimore, MD 21218, USA*

⁵*CREST, Japan Science and Technology Agency, Kawaguchi, Saitama 332-0012, Japan*

⁶*Trans-scale Quantum Science Institute, University of Tokyo, Bunkyo-ku, Tokyo 113-0033, Japan*

⁷*Materials Department, University of California,
Santa Barbara, Santa Barbara, California 93427, USA*

(Dated: January 30, 2025)

Magnetic rare earth atoms on pyrochlore lattice can produce such exotic magnetic states as spin ice and quantum spin ice. These states are a result of the frustration in the pyrochlore lattice, as well as crystal field degrees of freedom of rare earth atoms, and their interactions with the lattice. Raman scattering spectroscopy, which possess high spectral resolution and can easily access broad energy and temperature ranges, is an optimum tool to study these excitations and their interactions. In this work we follow Raman scattering of zone center phonons and crystal field excitations of Nd^{3+} in $\text{Nd}_2\text{Zr}_2\text{O}_7$ and $\text{Nd}_2\text{Ir}_2\text{O}_7$ in the temperature range where these materials are paramagnetic. A comparison between an insulating $\text{Nd}_2\text{Zr}_2\text{O}_7$ and semimetallic $\text{Nd}_2\text{Ir}_2\text{O}_7$ materials allow us to distinguish between scattering of phonons on other phonons, crystal field excitations, and electrons, highlighting interactions between these degrees of freedom.

I. INTRODUCTION

Frustrated 3D lattice of pyrochlores of a general formula $\text{A}_2\text{B}_2\text{O}_7$ with rare earth atoms at A site is known to host exotic magnetic states such as a spin ice, quantum spin ice states, and all-in-all-out (AIAO) order [1–3]. This research is still in its active phase, with the most understanding reached for the insulating pyrochlores. Recently, a new hope of finding a quantum spin liquid state appeared with the discovery of this state in a pyrochlore $\text{Ce}_2\text{Zr}_2\text{O}_7$ [4–7]. One of the compounds studied in this work, $\text{Nd}_2\text{Zr}_2\text{O}_7$, shows quantum spin-ice phase in the temperature regime above the ordering into AIAO state below $T_N \approx 0.3$ K [8, 9].

While materials with Zr on B cite are insulating, if a B site is occupied by Ir, its extended orbitals lead to semimetallic properties. A symmetry-protected quadratic band touching at Γ -point has drawn attention to these materials in the first place [10]. Since Ir is magnetic with $J=1/2$ and dominant antiferromagnetic interactions, Ir moments order at $T_N^{Nd} = 33$ K in AIAO order [11, 12]. This order breaks time reversal symmetry and can lead to a Weyl semimetal state [13–15], as was recently confirmed experimentally [16]. A combination of two magnetic sublattices, a rare earth on A site and Ir on B site, and an interplay or competition of various magnetic interactions leads to exotic magnetism of rare earth at elevated temperatures compared to the insulating pyrochlores, such as quantum-spin ice of Ho moments in $\text{Ho}_2\text{Ir}_2\text{O}_7$ [17] and proposed spin ice of Nd moments in $\text{Nd}_2\text{Ir}_2\text{O}_7$ at intermediate temperature [18], while the

ground state is AIAO order.

Understanding of interactions of the lattice with magnetic and electronic degrees of freedom in pyrochlores is an important way to fully understand the origin of the exotic magnetic and electronic states in these materials. A broad range of experimental and theoretical evidence of interactions of the lattice with magnetic degrees of freedom already exists, with those relevant to the studied compounds listed below. For rare-earth pyrochlores, interactions of lattice with dipole-octopole degree of freedom are exemplified experimentally and theoretically in $\text{Pr}_2\text{Zr}_2\text{O}_7$ [19] [and YBKim]. Modulation of crystal field excitations by phonons, so called vibronic coupling, is frequently observed in rare earth pyrochlores [20–22]. Exotic spin-phonon coupling mediated by spin-orbit coupling is suggested in pyrochlores with 5d atoms [23, 24]. Especially relevant to this study is the theoretical work which demonstrates how phonon Raman scattering can indirectly probe quantum spin-ice excitations [25]. Raman scattering spectroscopy, which probes Γ -point phonons with high spectral resolution, is a unique method to access this kind of information.

In this work we follow the temperature dependence of lattice phonons and crystal field excitations of two Nd-based pyrochlores, an insulating $\text{Nd}_2\text{Zr}_2\text{O}_7$ and a semimetallic $\text{Nd}_2\text{Ir}_2\text{O}_7$, in the high-temperature paramagnetic state. For $\text{Nd}_2\text{Zr}_2\text{O}_7$ we follow these excitations down to 10 K. For $\text{Nd}_2\text{Ir}_2\text{O}_7$ we follow them down to the temperature of AIAO ordering of Ir moments, $T_N^{Ir} = 33$ K, while the data in the magnetically ordered state are presented elsewhere [18]. While this temperature range is

above the temperatures of magnetic and electronic states which attracted the most attention to these materials, it provides an important insight into the interactions of the lattice with electronic excitations and crystal field excitations.

II. EXPERIMENTAL

$\text{Nd}_2\text{Ir}_2\text{O}_7$ single crystal was grown by the KF-flux method [26] and it has an as-grown octahedron-shaped (111) facet which was used for the measurements. $\text{Nd}_2\text{Zr}_2\text{O}_7$ single crystal was grown using floating zone technique [].

Raman scattering spectra were collected using the Jobin-Yvon T64000 triple monochromator spectrometer equipped with a liquid nitrogen cooled CCD detector. Measurements were performed in back-scattering geometry using micro-Raman channel equipped with an Olympus microscope, using laser probe of $2\mu\text{m}$ in diameter. 514.5 nm line of $\text{Ar}^+\text{-Kr}^+$ mixed gas laser was used as the excitation light.

For low temperature measurements, the samples were mounted on the cold-finger of Janis ST-500 cryostat, which can be cooled down to 4 K without laser heating. The laser power was kept at 0.5 mW for the measurements of $\text{Nd}_2\text{Zr}_2\text{O}_7$. Semimetallic $\text{Nd}_2\text{Ir}_2\text{O}_7$ has at least one order of magnitude lower Raman scattering signal. Therefore laser power of 2 mW was used for these measurements, which resulted in heating of the sample by 20 K. The temperatures presented in the paper are corrected for the laser heating

For the measurements, the large floating-zone-grown crystals of $\text{Nd}_2\text{Zr}_2\text{O}_7$ were oriented and cut, so that the Raman scattering measurements were taken from (001) plane with the polarization vector of the excitation laser $e \parallel a$, where a is crystallographic axis. Measurements were performed for (x, x) and (x, y) scattering channels. Measurements were done in the spectral range between 10-90 meV.

$\text{Nd}_2\text{Ir}_2\text{O}_7$ flux-grown crystals typically have pyramid shape with each direction less than 1 mm and naturally grown (111) facets. Raman scattering measurements were done from a cleaved surface of (111) facet of the crystal in $(x, x + y)$ scattering channel. Data in the spectral range from 10-90 meV were taken in the temperature range from 50 to 266 K. In order to obtain a temperature dependence for the phonons of $\text{Nd}_2\text{Ir}_2\text{O}_7$ in the broad temperature range despite a very low signal, the data were taken on continuous heating of the sample with a heating rate of 0.1 K/min. The data were averaged over 1 hour, which corresponds to averaging over 6 K. The averaging temperature range was selected in a way that the change in the spectra of the two successive averaging temperature ranges ΔT_1 and ΔT_2 was smaller than the noise amplitude A: $I(\Delta T_1) - I(\Delta T_2) < A$. Additionally, due to the small signal of $\text{Nd}_2\text{Ir}_2\text{O}_7$, data below 40 K were obtained using macro-channel of the

same spectrometer with a $50\mu\text{m}$ laser probe and pseudo-Brewster's angle incidence of the excitation light. More details about these data and electronic and magnetic scattering are presented elsewhere [16, 18].

All spectra were normalized on Bose-Einstein thermal population factor $[n(\omega) + 1]$, where $n(\omega)$ is the Bose occupation factor.

In order to obtain the temperature dependence of the phonon parameters demonstrated in Fig. 2, the phonon spectra were fit by a sum of Voigt lineshapes, where Gaussian component was kept 1.5 cm^{-1} in order to correct for the resolution of their spectrometer. The micro-channel Raman scattering measurements are known to introduce an artifact background for highly reflective samples with weak Raman response, which is true for $\text{Nd}_2\text{Ir}_2\text{O}_7$. To correctly analyze the Raman phonon scattering of $\text{Nd}_2\text{Ir}_2\text{O}_7$, which is the focus of this paper, we have identified the temperature-independent artifact background and subtracted it from all the data as a part of the primary data analysis. This background was identified in a following procedure: A spectrum at a given temperature was fit by a sum of Voigt lineshapes associated with the sharper features of phonons, and Gaussian lineshapes representing disordered background. Next, all Voigt fits were subtracted from the raw data to estimate a background. This background was fit to several new temperature independent Gaussians and a temperature dependent linear background. This total background was then subtracted from the raw spectra at each temperature to provide an excitation-only spectrum, devoid of any temperature independent background effects.

III. RESULTS

Figs. 1 and 3 presents temperature dependent Raman scattering spectra of $\text{Nd}_2\text{Zr}_2\text{O}_7$ in (x, x) and (x, y) scattering channels and $\text{Nd}_2\text{Ir}_2\text{O}_7$ in $(x, x + y)$ in 12- 70 meV spectral range, where we expect to observe phonons and crystal field excitations within the ground state $^4I_{9/2}$ multiplet. Dependence of the spectra on temperature and polarization allows to distinguish between phonons and crystal field excitations. Typically, sharp peaks observed already at room temperature are the excitations of Γ -point phonons, while crystal electric field (CEF) excitations appear in the spectra as well-defined peaks as the temperature is lowered due to large scattering at higher temperatures [27].

A. Phonon Raman scattering

Both $\text{Nd}_2\text{Zr}_2\text{O}_7$ and $\text{Nd}_2\text{Ir}_2\text{O}_7$ crystal structures belong to the $Fd\bar{3}m$ (No. 227) space group, which corresponds to O_h point group. Wickoff positions and respective Raman activity of the atoms is presented in Table I. This demonstrates that all the Raman-active phonons in these materials are related to the oxygen mo-

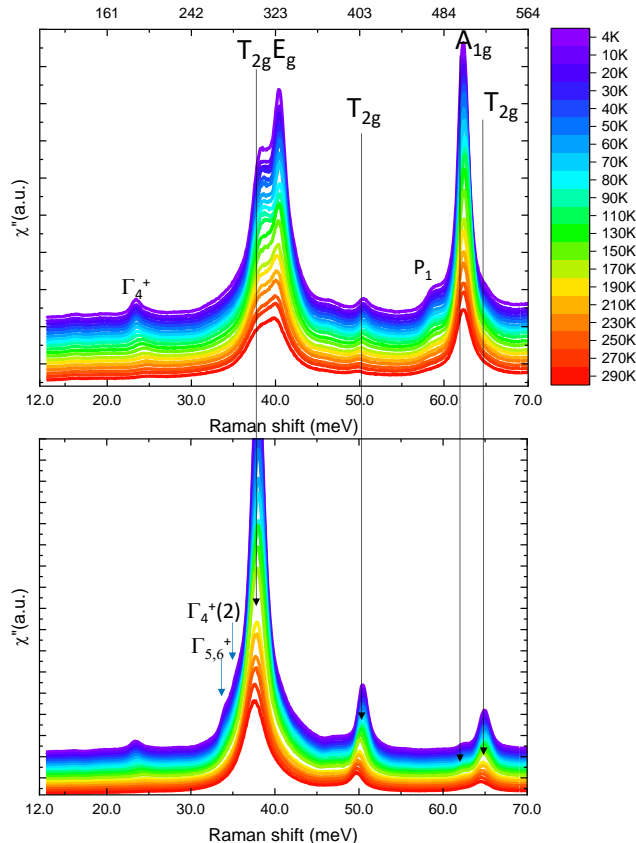


FIG. 1. Raman scattering spectra of $\text{Nd}_2\text{Zr}_2\text{O}_7$ between 290 and 15 K, upper panel shows (x, x) scattering channel, lower panel shows (x, y) scattering channel.

tion. Phonons were assigned using polarization dependence as noted in Table II and following DFT calculations of phonons for $\text{Pr}_2\text{Zr}_2\text{O}_7$ and $\text{Pr}_2\text{Ir}_2\text{O}_7$ presented in [20, 28].

TABLE I. Wyckoff positions and Γ -point representations for $\text{Nd}_2\text{Zr}_2\text{O}_7$ and $\text{Nd}_2\text{Ir}_2\text{O}_7$.

Element	Wyckoff position	Γ representation
Nd	16c	Inactive
Zr/Ir	16d	Inactive
O	48f	$A_{1g} + E_g + 3T_{2g}$
O'	8a	T_{2g}

TABLE II. Components of Raman tensor for (x, x) and (x, y) polarizations.

Geometry	A_{1g}	E_g	T_{2g}
(x, x)	a^2	b^2	c^2
(x, y)	0	b^2	$\frac{2}{3}c^2$

TABLE III. Phonon frequencies of $\text{Nd}_2\text{Zr}_2\text{O}_7$ and $\text{Nd}_2\text{Ir}_2\text{O}_7$ with the assignment based on the polarization dependence and DFT calculations for $\text{Pr}_2\text{Zr}_2\text{O}_7$ and $\text{Pr}_2\text{Ir}_2\text{O}_7$ presented in [28]

$\text{Nd}_2\text{Zr}_2\text{O}_7$	$\text{Nd}_2\text{Ir}_2\text{O}_7$	assignment
309	307	$T_{2g}^{(1)}$
326	336	E_g
406	396	$T_{2g}^{(2)}$
472 w		P1
503	509	A_{1g}
522	552	$T_{2g}^{(3)}$

1. Phonons of $\text{Nd}_2\text{Zr}_2\text{O}_7$

Temperature dependent Raman phonon spectra of $\text{Nd}_2\text{Zr}_2\text{O}_7$ in (x, x) and (x, y) scattering channels are shown in Fig. 1. Phonons are assigned based on their polarization dependence, see Table II. Their frequencies together with their assigned symmetries are listed in Table III. $T_{2g}^{(1)}$ and E_g phonons have very close lying frequencies, but can be distinguished due to different intensities in (x, x) and (x, y) scattering channels. Parameters of the phonons show weak temperature dependence (Fig. 2). Crystal field excitations marked in Fig 1 will be discussed in Sect. III B. Feature marked as P1 at 472 cm^{-1} appears in the spectra in both scattering channels. To our best knowledge, it cannot be assigned neither to Raman active phonons nor to crystal field excitations calculated using single on approximation with D_{3d} symmetry of the Nd^{3+} site.

Temperature dependent parameters of the $\text{Nd}_2\text{Zr}_2\text{O}_7$ phonons obtained from the fit of the spectra by a sum of Voigt shapes are presented in Fig. 2. The overall hardening and narrowing of the phonons on cooling follows the standard behavior determined by contraction of the unit cell and decrease of phonon scattering. In the absence of scattering other than phonon-phonon one, the temperature dependence of scattering γ of Γ -point optical phonons typically follows the Klemens model [29]: $\gamma(T, \omega) = \gamma_0 + A(2n_B(\omega/2) + 1)$, where γ_0 is a temperature independent term determined by disorder, ω is the phonon frequency, and n_B is levels population at temperature T for $\omega/2$, $n_B(T) = e^{\frac{\omega}{2kT}}$. In Fig 2, solid lines show $\gamma(T)$ expected from the Klemens model. While the overall temperature dependence of phonons width follows the Klemens model, for all the phonons we observe a deviation from it at about 100 K, where the width exceeds the expected value, but then decreases again the follow the conventional curve. Frequencies of the phonons also point on 100 K as a characteristic temperature. The hardening for all the phonons is observed only down to 100 K. Below this temperature the dependence of phonon frequency for phonons at around 38 and 50 meV flattens, while the other three phonons soften on further cooling. This behavior demonstrates that some other factor beyond regular phonon-phonon scattering is important for

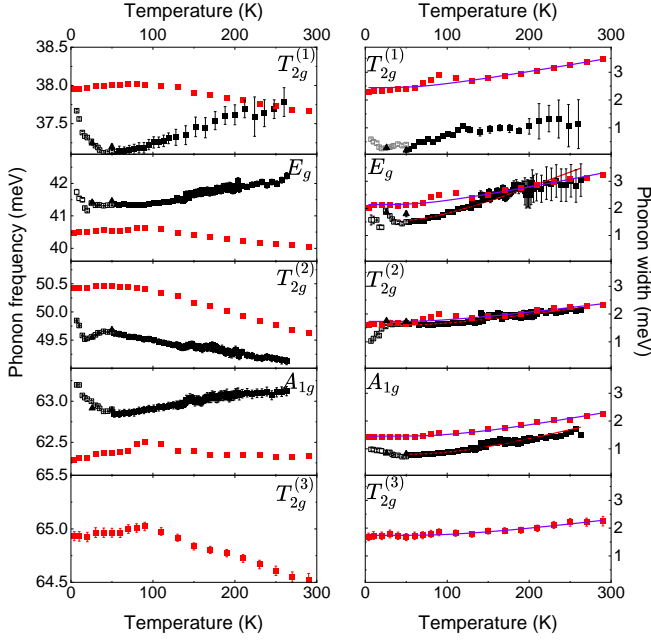


FIG. 2. Temperature dependence of frequencies (left panel) and width (right panel) of Raman active phonons in $\text{Nd}_2\text{Zr}_2\text{O}_7$ (red) and $\text{Nd}_2\text{Ir}_2\text{O}_7$ (blue and black). $\text{Nd}_2\text{Ir}_2\text{O}_7$ data is selected from polarization where phonon is most prominent, consistent with choices in Table V. In the right panel, solid lines show temperature dependence of phonon line width of $\text{Nd}_2\text{Zr}_2\text{O}_7$ (violet) and $\text{Nd}_2\text{Ir}_2\text{O}_7$ (red) suggested by the Klemens model of phonon-phonon scattering.

TABLE IV. Klemens model fit parameters for $\text{Nd}_2\text{Zr}_2\text{O}_7$, according to $\text{FWHM} = \gamma_0 + A(e^{\frac{\omega}{2k_bT}} - 1)^{-1}$. Selected fits are from polarization channel where phonon is most prominent.

Phonon	Polarization	ω (meV)	A (meV)	γ_0 (meV)
$T_{2g}^{(1)}$	XY	37.96	1.16	2.44
E_g	XX	40.49	1.46	2.14
$T_{2g}^{(2)}$	XY	50.42	1.11	1.73
A_{1g}	XX	62.29	2.08	1.46
$T_{2g}^{(3)}$	XY	64.93	1.44	1.74

the lattice response of $\text{Nd}_2\text{Zr}_2\text{O}_7$.

2. Phonons of $\text{Nd}_2\text{Ir}_2\text{O}_7$

Fig. 3 shows temperature dependent Raman spectra of $\text{Nd}_2\text{Ir}_2\text{O}_7$ in 35-70 meV spectral range in $(x, x+y)$ scattering channel in the paramagnetic state from room temperature down to 40 K. Since the structure of $\text{Nd}_2\text{Ir}_2\text{O}_7$ is very close to that of $\text{Nd}_2\text{Zr}_2\text{O}_7$ we expect phonons of the same symmetries and similar energies, despite the overall low intensity of the spectra. The comparison of frequencies of oxygen phonons for these two materials and the assignment is presented in Table III. We note that the

TABLE V. Klemens model fit parameters for $\text{Nd}_2\text{Ir}_2\text{O}_7$, according to $\text{FWHM} = \gamma_0 + A(e^{\frac{\omega}{2k_bT}} - 1)^{-1}$.

Phonon	ω (meV)	A (meV)	γ_0 (meV)
$T_{2g}^{(1)}$			
E_g	41.83	2.98	1.53
$T_{2g}^{(2)}$	49.31	1.24	1.60
A_{1g}	63.07	2.96	0.80
$T_{2g}^{(3)}$			

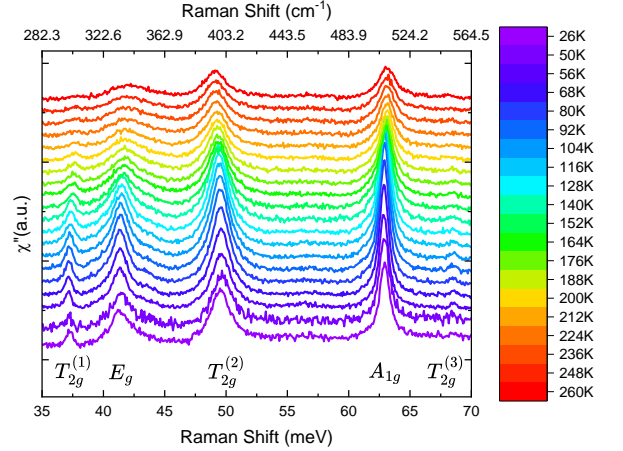


FIG. 3. Raman spectra of $\text{Nd}_2\text{Ir}_2\text{O}_7$ between 13 and 260 K in $(x, x+y)$ polarization

third T_{2g} mode can be observed as a small peak just below 70 meV, but the intensity is too weak for a discussion of its behavior beyond qualitative softening and narrowing upon cooling.

Temperature dependent parameters of the $\text{Nd}_2\text{Ir}_2\text{O}_7$ phonons are presented in Fig. 2. We can see that in contrast to $\text{Nd}_2\text{Zr}_2\text{O}_7$, the observed phonons soften upon cooling, except for the second T_{2g} mode which hardens. All the phonons narrow on lowering the temperature in the semimetallic state above T_N^{Ir} with the dependence which follows that of the Klemens model as shown by the red fitting curves in Fig. 2. Consistency with Klemens model is unclear for the first T_{2g} phonon, as the peak intensity is too small to precisely resolve the phonon linewidth. While at around 40 K the width of $\text{Nd}_2\text{Zr}_2\text{O}_7$ and $\text{Nd}_2\text{Ir}_2\text{O}_7$ phonons is nearly the same, the amplitude of the change is much larger for $\text{Nd}_2\text{Ir}_2\text{O}_7$ phonons, which show broader lines at room temperature. It suggests that similar to $\text{Nd}_2\text{Zr}_2\text{O}_7$ scattering is determined not only by the phonon-phonon scattering, however the origin of scattering is different. Below $T_N^{Ir}=33$ K the lattice responds to the TRS symmetry breaking due to AIAO order of Ir moments, and below 14 K to the ordering of Nd moments, the details are discussed elsewhere [18].

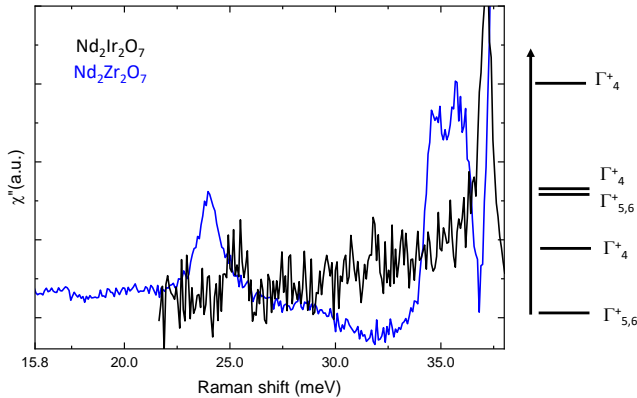


FIG. 4. (a) Lower frequency spectra in (x,y) channel at 160 and 14 K. The comparison reveals a wing of the phonon line in 14 K spectra, related to the CEF excitations (b) The subtraction reveals the doublet of CEF at 34 and 36 meV.

B. Crystal field excitation of Nd^{3+}

In addition to the excitations of the Γ -point phonons, in the measured frequency range we observe crystal field excitations of Nd^{3+} . The local symmetry of the Nd^{3+} , $J=9/2$, site in both structures is D_{3d} , which results in splitting of the orbital into five Kramers doublets (see Fig. 4) [30, 31]. For $\text{Nd}_2\text{Zr}_2\text{O}_7$, neutron scattering observed transitions at 23.4 meV, 35 meV and 106.2 meV. The transition observed at 35 meV was extra broad and thus assigned to the unresolved Γ_4^+ , $\Gamma_{5,6}^+$ doublet [31].

The transitions between the ground state and excited state doublets are expected to be observed in Raman scattering spectra. The doublet states for D_{3d} correspond to E_g point group symmetry, where $E_g \rightarrow E_g$ transitions will be observed in $E_g \otimes E_g = A_{1g} + A_{2g} + E_g$ scattering channels, meaning they will be visible in both (x,x) and (x,y) spectra for the studied pyrochlores. Regarding intensity of the crystal field excitations, our expectations are that it will be at least one order of magnitude lower than that of the oxygen phonons typically observed for pyrochlores, as was already demonstrated for $\text{Pr}_2\text{Ir}_2\text{O}_7$ and $\text{Pr}_2\text{Zr}_2\text{O}_7$ [20, 28]. One distinct property of CF excitations in Raman scattering which allows to distinguish them from other excitations is a strong temperature dependence of the scattering on temperature: As the result, these excitations are observed as sharp peak only at temperatures sufficiently lower than the energy of the excitation [27].

Due to the high overall intensity of Raman scattering in $\text{Nd}_2\text{Zr}_2\text{O}_7$, the lower frequency CF transitions can be relatively easily identified using the comparison between high and low temperature spectra. A peak at 23.5 meV of a transition from the ground state to the first excited state $\Gamma_{5,6}^+ \rightarrow \Gamma_4^+$ is well distinguished in the spectra below 160 K. CF in the range of 35 meV ap-

pear as a double “wing” of the strong $T_{2g}^{(1)}$ phonon band clearly observed in (x,y) channel (Fig. 1) on temperature lowering. Fig. 4 shows a result of subtraction of $\chi''(T=14\text{K}) - \chi''(300\text{K})$ in (x,y) channel for $\text{Nd}_2\text{Zr}_2\text{O}_7$. The doublet of excitations at 34.4 meV and 35.2 meV is revealed by the subtraction. These peaks correspond to the transitions from the ground state to the second and third excited states $\Gamma_{5,6}^+$ and Γ_4^+ , which were expected by calculations, and observed by neutron scattering as a single broad band [31].

Since the overall intensity of $\text{Nd}_2\text{Ir}_2\text{O}_7$ spectra is two orders of magnitude lower than that of $\text{Nd}_2\text{Zr}_2\text{O}_7$, detecting crystal field excitations becomes a challenge. Thus we can observe clearly only the excitation to the first excited state $\Gamma_{5,6}^+ \rightarrow \Gamma_4^+$ found at at 25.3 meV (see Fig. 4). This spectrum obtained by averaging $\chi''(T) - \chi''(263\text{K})$ for the temperatures between 50 and 90 K, using the fact that crystal field excitations show basically no temperature dependence on their frequencies. This is in agreement with neutron scattering measurements for $\text{Nd}_2\text{Ir}_2\text{O}_7$, where transitions at 26 meV and 41 meV were observed, with the second peak being broader [30]. In our Raman scattering measurements the transitions to the second excited states couldn’t be distinguished from the phonon scattering.

IV. DISCUSSION

The temperature dependence of the Raman-active Γ -point phonons in $\text{Nd}_2\text{Zr}_2\text{O}_7$ and $\text{Nd}_2\text{Ir}_2\text{O}_7$ suggests that in both compounds the lattice is interacting with the other degrees of freedom and the scattering of phonons is determined by factors beyond phonon-phonon scattering as described by the Klemens model. The comparison highlights the dominance of different scattering channel for the insulating $\text{Nd}_2\text{Zr}_2\text{O}_7$ versus semimetallic $\text{Nd}_2\text{Ir}_2\text{O}_7$.

In $\text{Nd}_2\text{Zr}_2\text{O}_7$ frequencies of the phonons harden on cooling down to approximately 100 K, and either stay temperature independent, or soften on cooling below this temperature, with the softening the most pronounced for $T_{2g}^{(3)}$ phonon. The observed hardening of the phonons down to 100 K is in the agreement with the decrease of the lattice constant a on cooling [29, 31]. The temperature dependence of the width of the phonons follows the shape determined by the phonon-phonon scattering as expected by the Klemens model [29], but deviates from it around 100 K, suggesting an additional scattering channel in this relatively narrow temperature range. This characteristic temperature range around 100 K was also identified in $\text{Nd}_2\text{Zr}_2\text{O}_7$ heat capacity measurements [31, 32] as a broad feature of a Schottky-like anomaly. It was interpreted as magnetic contribution associated with the depopulation of the first excited crystal field level at 24 meV. It is natural to assign the feature in the heat capacity and in the temperature dependence of the phonon scattering to the same effect, pointing on the

scattering of phonons on crystal field excitations. The scattering of the crystal field excitations on the phonons is a known effect [27]. To our best knowledge the effect on the scattering of the phonons has never been detected yet, with the $\text{Nd}_2\text{Zr}_2\text{O}_7$ apparently providing the optimum system to detect this effects due to the convenient temperature scale [27]. While scattering of phonons on crystal field excitations is not discussed explicitly, this effect points on scattering channels of magnetic origin which can exist for phonons in rare-earth pyrochlores [25]

The large width of $\text{Nd}_2\text{Ir}_2\text{O}_7$ phonons at room temperature compared to other pyrochlore iridates for which the data are available [28, 33–35] and the unusually large decrease of scattering with lowering the temperature also suggests scattering beyond the phonon-phonon one. Similarly to $\text{Pr}_2\text{Ir}_2\text{O}_7$, we suggest that electron-phonon scattering is the dominant process [28, 34]: A decrease of scattering occurs due to the relevant electronic levels depopulation on cooling. Both in $\text{Nd}_2\text{Ir}_2\text{O}_7$ and $\text{Pr}_2\text{Ir}_2\text{O}_7$ the phonons are only broad at high temperatures, with their scattering decreases below about 150 K. Interestingly, this temperature range around 150 K is close to the temperature range where other iridates go through the metal insulator transition.

Of a special interest is the comparison of our results on Nd-based materials with Pr-based ones. Our previous Raman scattering studies of Pr-based compounds demonstrated a splitting of the E_g phonon in $\text{Pr}_2\text{Zr}_2\text{O}_7$ and an extreme broadening of this phonon in $\text{Pr}_2\text{Ir}_2\text{O}_7$, which cannot be explained by vibronic coupling [20, 28]. In contrast, E_g phonons in Nd-based pyrochlores studied here do not show any splitting or broadening different from that of T_{2g} phonons. A coupling of the E_g lattice degree of freedom with magnetic degree of freedom in non-Kramers pyrochlores, which does not require an overlap of energies of magnetic excitations and phonons, suggested in Ref. [25], can provide an explanation for our observations. The respective splitting of the ground state crystal field level in $\text{Pr}_2\text{Zr}_2\text{O}_7$ has been detected by neutron scattering [36] and Raman scattering spectroscopy [20] at low temperatures. $\text{Pr}_2\text{Ir}_2\text{O}_7$ can possess similar properties, however the overlap in the spectral range with electronic scattering prevents the detection of the relevant crystal field transitions [16]. The detection of the coupling proposed in Ref. [25] in the high-temperature paramagnetic regime of the rare earth pyrochlores can be the first step to the identification the scattering on the excitations in quantum spin ice state of these materials.

While the phonon behavior of these two materials shows unexpected behavior, crystal field levels follow the calculated energies [31]. For $\text{Nd}_2\text{Zr}_2\text{O}_7$ Raman scattering measurements allow to resolve the expected from the calculation doublet of transitions to the second and third

excited states $\Gamma_{5,6}^+$ and Γ_4^+ at 34.4 meV and 35.2 meV. For $\text{Nd}_2\text{Ir}_2\text{O}_7$, due to very low intensities of the spectra in a semimetal and an overlap with the phonons, we can only identify a position of the first excited state. The width of the excitation is similar to that of $\text{Nd}_2\text{Zr}_2\text{O}_7$, suggesting that the lifetime of these localized excitations are not much affected by the difference in the electronic structure of the materials

V. CONCLUSIONS

In this work we present the evolution of phonon and crystal field Raman scattering in $\text{Nd}_2\text{Zr}_2\text{O}_7$ and $\text{Nd}_2\text{Ir}_2\text{O}_7$ on lowering temperature in the temperature range where both materials are paramagnetic. We demonstrate that $\text{Nd}_2\text{Zr}_2\text{O}_7$ the lattice reacts to the depopulation of the lowest crystal field level, providing an additional scattering channel for phonons in the relevant temperature range, in addition to the phonon-phonon scattering described by Klemens model. A correlation between thermal contraction and CEF levels depopulation also points on the coupling with between these two degrees of freedom in $\text{Nd}_2\text{Zr}_2\text{O}_7$ their as an additional factor determining the behavior of crystal lattice in paramagnetic state. Raman scattering spectra allow to measure positions of CEF in $\text{Nd}_2\text{Zr}_2\text{O}_7$ with high precision and resolve a doublet which was expected from the calculations.

Two lower frequency $\text{Nd}_2\text{Ir}_2\text{O}_7$ phonons ($T_{2g}^{(1)}$ and E_g) experience dramatic decrease of scattering on cooling from room temperature down to T_N^{Nd} . We interpret this as a consequence of electron-phonon scattering and the decrease of the thermal population of relevant electronic levels around 150 K.

ACKNOWLEDGMENTS

The authors are thankful to Y. Yang for useful discussions. This work at the Institute for Quantum Matter was funded by the U.S. Department of Energy, Office of Science, Basic Energy Sciences under Awards No. DE-SC0019331 and DE-SC0024469. This work was partially supported by JST-MIRAI Program (JPMJMI20A1), JST-ASPIRE Program (JPMJAP2317) and by the fund made by Canadian Institute for Advanced Research. SDW and EZ acknowledge support from the US Department of Energy (DOE), Office of Basic Energy Sciences, Division of Materials Sciences and Engineering under Grant No. DE-SC0017752. SDW and EZ's work used facilities supported via the UC Santa Barbara NSF Quantum Foundry funded via the Q-AMASE-i program under award DMR-1906325.

[1] J. S. Gardner, M. J. P. Gingras, and J. E. Greedan, *Rev. Mod. Phys.* **82**, 53 (2010).

[2] M. J. Gingras and P. A. McClarty, *Reports on Progress*

- in Physics **77**, 056501 (2014).
- [3] J. G. Rau and M. J. Gingras, Annual Review of Condensed Matter Physics **10**, 357 (2019).
- [4] J. Gaudet, E. M. Smith, J. Dudemaine, J. Beare, C. R. C. Buhariwalla, N. P. Butch, M. B. Stone, A. I. Kolesnikov, G. Xu, D. R. Yahne, K. A. Ross, C. A. Marjerrison, J. D. Garrett, G. M. Luke, A. D. Bianchi, and B. D. Gaulin, Phys. Rev. Lett. **122**, 187201 (2019).
- [5] B. Gao, T. Chen, D. W. Tam, C.-L. Huang, K. Sasmal, D. T. Adroja, F. Ye, H. Cao, G. Sala, M. B. Stone, *et al.*, Nature Physics **15**, 1052 (2019).
- [6] E. M. Smith, O. Benton, D. R. Yahne, B. Placke, R. Schäfer, J. Gaudet, J. Dudemaine, A. Fitterman, J. Beare, A. R. Wildes, S. Bhattacharya, T. DeLazzer, C. R. C. Buhariwalla, N. P. Butch, R. Movshovich, J. D. Garrett, C. A. Marjerrison, J. P. Clancy, E. Kermarrec, G. M. Luke, A. D. Bianchi, K. A. Ross, and B. D. Gaulin, Phys. Rev. X **12**, 021015 (2022).
- [7] A. Bhardwaj, S. Zhang, H. Yan, R. Moessner, A. H. Nevidomskyy, and H. J. Changlani, npj Quantum Materials **7**, 51 (2022).
- [8] M. Léger, E. Lhotel, M. Ciomaga Hatnean, J. Ollivier, A. R. Wildes, S. Raymond, E. Ressouche, G. Balakrishnan, and S. Petit, Phys. Rev. Lett. **126**, 247201 (2021).
- [9] J. Xu, O. Benton, A. Islam, T. Guidi, G. Ehlers, and B. Lake, Physical Review Letters **124**, 097203 (2020).
- [10] W. Witczak-Krempa and Y. B. Kim, Phys. Rev. B **85**, 045124 (2012).
- [11] K. Matsuhira, M. Wakeshima, Y. Hinatsu, and S. Takagi, Journal of the Physical Society of Japan **80**, 094701 (2011).
- [12] K. Ueda, J. Fujioka, Y. Takahashi, T. Suzuki, S. Ishiwata, Y. Taguchi, and Y. Tokura, Phys. Rev. Lett. **109**, 136402 (2012).
- [13] X. Wan, A. M. Turner, A. Vishwanath, and S. Y. Savrasov, Physical Review B **83**, 205101 (2011).
- [14] W. Witczak-Krempa, G. Chen, Y. B. Kim, and L. Balents, Annual Review of Condensed Matter Physics **5**, 57 (2014).
- [15] L. Savary and L. Balents, Reports on Progress in Physics **80**, 016502 (2016).
- [16] P. Nikolić, Y. Xu, T. Ohtsuki, D. C. Elbert, S. Nakatsuji, and N. Drichko, Phys. Rev. B **110**, 035148 (2024).
- [17] M. J. Pearce, K. Götze, A. Szabó, T. Sikkenk, M. R. Lees, A. Boothroyd, D. Prabhakaran, C. Castelnovo, and P. Goddard, Nature Communications **13**, 444 (2022).
- [18] Y. Xu, Y. Yang, J. Teyssier, T. Ohtsuki, Y. Qiu, S. Nakatsuji, D. van der Marel, N. B. Perkins, and N. Drichko, arXiv preprint arXiv:2302.00579 (2023).
- [19] N. Tang, Y. Gritsenko, K. Kimura, S. Bhattacharjee, A. Sakai, M. Fu, H. Takeda, H. Man, K. Sugawara, Y. Matsumoto, *et al.*, Nature Physics **19**, 92 (2023).
- [20] Y. Xu, H. Man, N. Tang, S. Baidya, H. Zhang, S. Nakatsuji, D. Vanderbilt, and N. Drichko, Phys. Rev. B **104**, 075125 (2021).
- [21] J. Gaudet, A. M. Hallas, C. R. C. Buhariwalla, G. Sala, M. B. Stone, M. Tachibana, K. Baroudi, R. J. Cava, and B. D. Gaulin, Phys. Rev. B **98**, 014419 (2018).
- [22] P. Thalmeier and P. Fulde, Physical Review Letters **49**, 1588 (1982).
- [23] C. H. Sohn, C. H. Kim, L. J. Sandilands, N. T. M. Hien, S. Y. Kim, H. J. Park, K. W. Kim, S. Moon, J. Yamaura, Z. Hiroi, *et al.*, Physical Review Letters **118**, 117201 (2017).
- [24] J. Son, B. C. Park, C. H. Kim, H. Cho, S. Y. Kim, L. J. Sandilands, C. Sohn, J.-G. Park, S. J. Moon, and T. W. Noh, npj Quantum materials **4**, 17 (2019).
- [25] A. Seth, S. Bhattacharjee, and R. Moessner, Phys. Rev. B **106**, 054507 (2022).
- [26] J. N. Millican, R. T. Macaluso, S. Nakatsuji, Y. Machida, Y. Maeno, and J. Y. Chan, Materials research bulletin **42**, 928 (2007).
- [27] M. Cardona and G. Güntherodt, *Light Scattering in Solids VII: Crystal-Field and Magnetic Excitations*, Vol. 75 (Springer, 2000).
- [28] Y. Xu, H. Man, N. Tang, T. Ohtsuki, S. Baidya, S. Nakatsuji, D. Vanderbilt, and N. Drichko, Phys. Rev. B **105**, 075137 (2022).
- [29] Y. Kim, X. Chen, Z. Wang, J. Shi, I. Miotkowski, Y. Chen, P. Sharma, A. Lima Sharma, M. Hekmaty, Z. Jiang, *et al.*, Applied Physics Letters **100**, 071907 (2012).
- [30] M. Watahiki, K. Tomiyasu, K. Matsuhira, K. Iwasa, M. Yokoyama, S. Takagi, M. Wakeshima, and Y. Hinatsu, in *Journal of Physics: Conference Series*, Vol. 320 (IOP Publishing, 2011) p. 012080.
- [31] J. Xu, V. K. Anand, A. K. Bera, M. Frontzek, D. L. Abernathy, N. Casati, K. Siemensmeyer, and B. Lake, Phys. Rev. B **92**, 224430 (2015).
- [32] M. Hatnean Ciomaga, M. R. Lees, O. A. Petrenko, D. S. Keeble, G. Balakrishnan, M. J. Gutmann, V. V. Klekovkina, and B. Z. Malkin, Phys. Rev. B **91**, 174416 (2015).
- [33] K. Ueda, R. Kaneko, A. Subedi, M. Minola, B. J. Kim, J. Fujioka, Y. Tokura, and B. Keimer, Phys. Rev. B **100**, 115157 (2019).
- [34] M. Rosalin, P. Telang, S. Singh, D. V. S. Muthu, and A. K. Sood, Phys. Rev. B **108**, 195144 (2023).
- [35] M. Rosalin, P. Telang, S. Singh, D. Muthu, and A. Sood, Physical Review B **109**, 184434 (2024).
- [36] J.-J. Wen, S. M. Koohpayeh, K. A. Ross, B. A. Trump, T. M. McQueen, K. Kimura, S. Nakatsuji, Y. Qiu, D. M. Pajerowski, J. R. D. Copley, and C. L. Broholm, Phys. Rev. Lett. **118**, 107206 (2017).